International Journal of Rock Mechanics & Mining Sciences 59 (2013) 179–190

Contents lists available at SciVerse ScienceDirect

International Journal of Rock Mechanics & Mining Sciences

journal homepage: www.elsevier.com/locate/ijrmms

Numerical modeling on destress blasting in coal seam for enhancing gas drainage

W.C. Zhu *, C.H. Wei, S. Li, J. Wei, M.S. Zhang

Key Laboratory of Ministry of Education on Safe Mining of Deep Metal Mines, Northeastern University, Shenyang 110819, China

ARTICLE INFO

Article history:
Received 6 August 2011
Received in revised form
30 July 2012
Accepted 3 November 2012
Available online 28 February 2013

Keywords:
Coal seam
Destress blasting
Gas drainage
Blasting stress wave
Blasting damage
Numerical simulation

ABSTRACT

Controlled blasting for loosening coal seams is one of the most important measures to enhance gas drainage and thus prevent coal and gas outbursts. The formation and development of blasting-induced damage zone, as well as the gas flow in damaged coal seams, can be considered as a coupled process among gas flow, solid deformation and damage. In this work, a coupled multiphysical model for the interaction between blasting damage of coal seam and gas flow is proposed, based on which, the effect of destress blasting on draining gas in coal seam is numerically simulated and the associated mechanisms for enhanced gas drainage induced by blasting damage are clarified. The loosening of coal seam induced by blasting is considered as a damage process that is dominated by the combined contribution of blasting stress wave and blasting-induced gas pressure, in this respect, the blasting damage of rock and coal seam is numerically simulated and compared with the existing experimental observations. Then, by considering the effect of coal seam damage on the gas permeability, the gas drainage enhanced by blasting damage is quantified based on the numerical simulations. It is demonstrated that the blasting damage around the borehole can not only alleviate the stress concentration at the perimeter of the borehole but also enhance the gas drainage due to the increase of the gas permeability in the damaged coal seam.

1. Introduction

Coal and gas outbursts have created serious difficulties for the coal mining industry around the world, leading to high intensity research efforts, large expenditures, and determined attempts to improve the various ventilation and gas drainage technique [1]. In this regard, improved solutions, such as the optimization of drainage systems and measures for the control of gas emissions during mining operations, are still needed to be found in order to predict and prevent the coal and gas outbursts [2]. High gas content is one of the most important factors that controls the coalbed methane productivity, however, it does not necessarily guarantee high production rate when permeability is too low, which is the case that is usually encountered in many coal fields of China [3]. The most commonly applied methane control solution, especially in high in-place gas content coalbed, is drilling methane drainage boreholes into the panel area prior to longwall mining to reduce the methane content of the coalbed [4]. The coal seam is generally affected by the complex geological conditions, such as low permeability and low saturation, the hydraulic fracturing, waterjet and controlling blasting are usually implemented in order to increase the permeability of coal seam and enhance the gas drainage. During the hydraulic fracturing the creation of the fractures is generally affected by the in-situ geo-stress conditions [5]. High-pressure waterjets are utilized to create artificial factures in specific directions within the existing gas drainage borehole and form fractural networks in a panel [3]. When high-pressure pulsed waterjet impacts the coal seam with high speed, the stress wave will be triggered, which may also enhance the coal permeability [6].

In addition, the controlling blasting, for example, pre-splitting blasting, or destress blasting is usually utilized to induce the damage in the coal seam. Destress blasting in one of the tools to improve mine safety and it is one of the most valuable techniques to control the damaging effects of rockbursts. [7]. Konicek et al. [8] presented a state-of-the-art review of destress blasting in coal mining, and discussed the effectiveness of destress blasting as a measure to overcome the challenges of high mining-induced stresses causing coal bumps and rockbursts. Andrieuxa and Hadjigeorgiou [9] focused on destress blasting as a technique for reducing ground stresses in underground mines in order to alleviate or mitigate the effects of rockbursts, which provided a series of easily implemented steps that result in a rational assessment of the likelihood of success of a given destress blast design in a given situation of rock mass conditions and stress regime. The pre-splitting blasting was thought to be an effective

* Corresponding author. Tel.: +86 24 83687705; fax: +86 24 83681186.
E-mail address: zhuwancheng@mail.neu.edu.cn (W.C. Zhu).

1365-1609/$ - see front matter © 2012 Elsevier Ltd. All rights reserved.
http://dx.doi.org/10.1016/j.ijrmms.2012.11.004

measure to enhance the pre-drainage rate of gas in low permeability coal seam [10]. Hydraulic fracturing after water-pressure controlled blasting was also adopted to increase the number and range of hydraulic cracks and improve the permeability of coal seams [11].

During the destress blasting, the detonating of explosive results in two types of loadings applied on the borehole wall, namely a stress wave pulse and a explosion gas pressure with longer duration. The stress wave is responsible for initiation of the crushing zone and the surrounding radial fractures, while the explosion gas pressure further extends the fractures [12,13]. In the blasting practice, the waveform should be regulated in order to control the fractures around the cavity.

In this respect, in order to examine the gas extraction in damaged coal seam induced by destress blasting, the formation of blasting damaged zone, together with the subsequent gas migration in coal seam should be considered as a fully coupled process among gas flow, deformation and damage of coal seam. In the past several decades, many attempts have been made in the numerical simulations of blasting-induced damage and gas drainage in coal seam, respectively [2,12–21]. Karacan et al. [21] investigated the different horizontal methane drainage borehole patterns, borehole lengths, and degasification times prior to and during the panel extraction to evaluate their effectiveness in reducing methane emission using a 3D reservoir modeling of a longwall panel. The Lunagas 'Floorgas' and 'Roofgas' are PC based computer programs that developed based on boundary element method for the simulations of strata relaxation and gas release phenomena associated with underground mining activities [1], which offer an effective tool for improving the accuracy and quality of gas control, gas capture technologies and ventilation system design. However, up to now, what is not understood is that the associated mechanism during the gas drainage in the coal seam that is damaged and distressed by blasting, when it is examined as a whole process that is combined with the damage of coal seam and gas flow in the damaged coal seam.

To this end, in this work, a coupled coal-gas model for the interaction between blasting damage of coal seam and gas flow is proposed, based on which, the evolution of damaged zone and coal seam stress near the working face before and after destress blasting is examined by means of numerical simulation. Finally, the effect of destress blasting on draining gas in coalbed is detailed.

2. Assignment of material properties

In order to characterize the heterogeneity of geo-materials such as rock, concrete and coal, in this study, the geo-material is assumed to be composed of many mesoscopic elements, and the mechanical properties of these elements are assumed to conform to a given Weibull distribution as defined in the following probability density function [22]

$$f(u)=\frac{m}{u_0}\left(u/u_0\right)^{m-1}\exp\left[-\left(u/u_0\right)^m\right] \tag{1}$$

where u is the mechanical parameter of the element (such as strength or elastic modulus); the scale parameter u_0 is related to the average of the element parameters and the parameter m defines the shape of the distribution function. From the properties of the Weibull distribution, a larger value of m implies a more homogeneous material and vice versa. Therefore, the parameter m is called the homogeneity index. For higher values of the homogeneity index, the strengths of more elements are concentrated closer to u_0. An increase in homogeneity index leads to more homogeneous numerical specimen. Using Eq. (1) in a computer simulation of a medium composed of many mesoscopic elements, one can produce numerically a heterogeneous geo-material specimen. The computationally produced heterogeneous specimen is analogous to a real specimen tested in the laboratory, so in this investigation it is referred to as a numerical specimen. In this respect, the influence of heterogeneity of material properties on coupled process can be examined based on the numerical simulations.

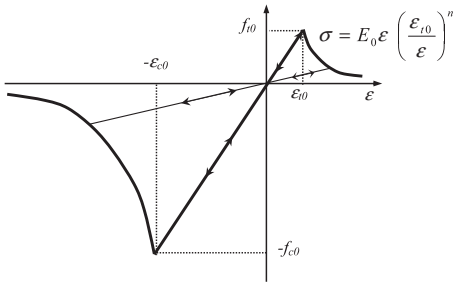

Fig. 1. The elastic damage-based constitutive law under uniaxial stress condition.

3. Governing equations

The present study will involve two coupled processes that are blasting damage of coal seam and gas flow in damaged coal seam, where one physical process affects the initiation and progress of the other. In this study, conservation equations for mass and momentum are derived on the macroscopic scale (all variables are averaged over the REV of the medium) for a saturated, porous elastic medium (coal seam).

3.1. Mechanical equilibrium and damage evolution equation

Initially the porous medium is assumed elastic, with constitutive relationship defined by a generalized Hooke's law. In this regard, a modified Navier's equation, in terms of displacement under a combination of changes of applied stresses (positive for tension) and gas pressures p (negative for suction) is expressed as

$$Gu_{i,jj}+\frac{G}{1-2\nu}u_{j,ji}-\alpha p_{,i}+F_i=\rho_s\frac{\partial^2 u_i}{\partial t^2}, \tag{2}$$

where u_i ($i=x, y, z$) is displacement (m), t is time (s), ρ_s is rock density (kg/m^3), G is shear modulus (Pa), ν is the Poisson's ratio, F_i is the component of the net body force in the i-direction (N/m^3), and the parameter α (≤ 1) is Biot's coefficient. This equation expresses the mechanical equilibrium in porous media subjected to dynamic loading where the effect of fluid pressure is taken into account according to effective stress law.

As illustrated in Fig. 1, the damage of medium in tension or shear is initiated when its state of stress satisfies the maximum tensile stress criterion or the Mohr–Coulomb criterion, respectively, as expressed by [22]

$$F_1\equiv\sigma_1-f_{t0}=0 \text{ or } F_2\equiv-\sigma_3+\sigma_1[(1+\sin\theta)/(1-\sin\phi)]-f_{c0}=0 \tag{3}$$

where f_{t0} and f_{c0} are uniaxial tensile and compressive strengths (Pa), respectively, θ is internal frictional angle, and F_1 and F_2 are two damage threshold functions.

According to the elastic damage theory, the elastic modulus of an element degrades monotonically as damage evolves, and the elastic modulus of damaged material is expressed as follows:

$$E=(1-D)E_0 \tag{4}$$

where D represents the damage variable, and E and E_0 are the elastic moduli of the damaged and the undamaged material (Pa), respectively. In this kind of numerical simulation, the element as well as its damage is assumed isotropic, so the E, E_0 and D are all scalars. Under any stress conditions, the tensile stress criterion is applied preferentially. According to Fig. 1, the damage variable can be calculated as

$$D=\begin{cases} 0 & F_1<0 \quad \text{and} \quad F_2<0 \\ 1-\left|\frac{\varepsilon_{t0}}{\varepsilon_1}\right|^n & F_1=0 \quad \text{and} \quad dF_1>0 \\ 1-\left|\frac{\varepsilon_{c0}}{\varepsilon_3}\right|^n & F_2=0 \quad \text{and} \quad dF_2>0 \end{cases} \tag{5}$$

where ε_{t0} and ε_{c0} are maximum tensile principal strain and maximum compressive principal strain when damage occurs, and n is a constitutive coefficient and it is 2.0. In this respect, the damage variable calculated with Eq. (5) is always from 0 to 1.0 regardless of what kind of damage it may suffer. It should be noted that, in the numerical implementation of Eq. (5), the tensile damage is always preferable to shear one, that is to say, the maximum tensile stress criterion is first used to judge whether the elements damage in tension or not, only the elements that do not damage in tensile mode will be checked for its shear damage with the Mohr–Coulomb criterion.

3.2. Gas flow equation

The coal is composed of a solid matrix that contains interstitial pore space filled with a freely diffusing pore gas. The absorption or desorption of gas may occur when the gas pressure and porosity of coal seam are changed. The gas flow equation in coal can be written as [19]

$$\beta\left[\frac{\phi}{p_0}+\frac{a_1a_2\rho_s}{1+a_2p}-\frac{a_1a_2^2\rho_sp}{2(1+a_2p)^2}\right]\frac{\partial p^2}{\partial t}-\nabla\left(\beta\frac{k}{\mu_g}\nabla p^2\right)=Q_g \tag{6}$$

where p is gas pressure (Pa), β is a compressibility factor ($\mathrm{kg\cdot m^{-3}\,Pa^{-1}}$), ϕ is porosity, p_0 is unit atmospheric pressure (1.013×10^5 Pa), a_1 and a_2 are Langmuir's constants with units of $\mathrm{m^3\,kg^{-1}}$ and $\mathrm{Pa^{-1}}$, respectively, μ_g is gas dynamic viscosity (Pa s), k is gas permeability of coal seam ($\mathrm{m^2}$), Q_g is source term ($\mathrm{kg\,m^{-3}\,s^{-1}}$), and t is time (s).

The effect of fluid flow on the mechanical process is implicit in Eq. (2). On the other hand, the porosity is closely dependent on the stress conditions, which is given as [19]

$$\phi=(\phi_0-\phi_r)\exp(\alpha_\phi\sigma_v)+\phi_r \tag{7}$$

where ϕ_0 is porosity at zero stress, α_ϕ is stress sensitivity coefficient, which is $5.0\times10^{-8}\,\mathrm{Pa^{-1}}$, ϕ_r is residual porosity at high stress and σ_v is the effective mean stress (with tension positive and in Pa), which is calculated as $\sigma_v=(\sigma_1+\sigma_2+\sigma_3)/3+\alpha p$, where σ_1, σ_2 and σ_3 are first, second and third principal stresses (Pa), respectively.

Besides, the permeability is correlated to the porosity according to the following exponential function

$$k=k_0(\phi/\phi_0)^3\exp(\alpha_kD) \tag{8}$$

where k_0 is the zero-stress permeability ($\mathrm{m^2}$), α_k is 5.0 called damage-permeability effect coefficient to indicate the effect of damage on the permeability, and D is damage variable that can be calculated according to Eq. (5).

3.3. Boundary conditions

Stress–displacement conditions for the mechanical analysis are defined as

$$\mathbf{u}(\mathbf{x},t)=\overline{\mathbf{u}}(\mathbf{x},t), \quad t\in[0,\infty), \tag{9}$$

$$\sigma(\mathbf{x},t).\mathbf{n}=\overline{\mathbf{F}}(\mathbf{x},t), \quad t\in[0,\infty), \tag{10}$$

where $\overline{u}(\mathbf{x},t)$ and $\overline{\mathbf{F}}(\mathbf{x},t)$ are the known displacement and stress at boundary, respectively, and $\mathbf{n}$ is the outward unit normal vector on the domain boundary.

Gas flow process:

The Dirichlet condition:

$$p(\mathbf{x},t)=\overline{p}(\mathbf{x},t), \quad t\in[0,\infty), \tag{11}$$

The Neumann condition

$$\frac{\mathbf{k}}{\mu_g}\nabla p\cdot n=\overline{Q}_l(\mathbf{x},t), \quad t\in[0,\infty), \tag{12}$$

where $\overline{p}(\mathbf{x},t)$ and $\overline{Q}_l(\mathbf{x},t)$ are known boundary gas pressure and gas flux, respectively.

3.4. Initial conditions

Initial conditions for the mechanical, flow and thermal analyses are defined as

$$\mathbf{u}(\mathbf{x},0)=\mathbf{u}_0 \text{ on } V, \tag{13}$$

$$\sigma(\mathbf{x},0)=\boldsymbol{\sigma}_0 \text{ on } V, \tag{14}$$

$$p(\mathbf{x},0)=p_0 \text{ on } V, \tag{15}$$

where $\boldsymbol{u}_0$, $\boldsymbol{\sigma}_0$ and p_0 are initial values of displacement, stress and gas pressure at the domain V. The quantity V represents the volume under consideration.

The above governing Eqs. (2)–(8), especially the mechanical equilibrium (Eq. (2)) and gas flow equation (Eq. (6)) are nonlinear partial differential equations (PDEs) with second order for space and first order for time. The non-linearity appears both in space and time domain, and therefore these equations are not possible to solve theoretically. In this respect, the complete set of coupled equations is implemented into, and solved by using COMSOL Multiphysics, a powerful PDE-based multiphysics modeling environment [23].

In COMSOL Multiphysics, the specified PDEs may be non-linear and time dependent and act on a 1D, 2D or 3D geometry. The PDEs and boundary values that are represented by general forms is

$$\begin{cases} d_a\frac{\partial u_l}{\partial t}+\nabla\cdot\Gamma_l=F_l & \text{in } \Omega & 16(a) \\ -\mathbf{n}\cdot\Gamma_l=G_l+\left(\frac{\partial R_m}{\partial u_l}\right)\mu_m & \text{on } \partial\Omega & 16(b) \\ 0=R_m & \text{on } \partial\Omega & 16(c) \end{cases}$$

The first Eq. (16a) is satisfied inside the domain Ω, and the second (16b) (generalized Neumann boundary) and third (16c) (Dirichlet boundary) equations are both satisfied on the boundary of the domain ∂Ω. $\mathbf{n}$ is the outward unit normal and is calculated internally. The equation index l ranges from 1 to N, while the constraint index m ranges from 1 to M. This discussion uses the summation convention. F_l, G_l, and R_m are scalars and can be functions of the space, time, and the solution u_l, whereas Γ_l is a vector and μ_m ($m=1, 2, \ldots, M$) are unknown vector-valued functions called Lagrange multipliers [23]. This multiplier is also calculated internally and will only be used in the case of mixed boundary conditions.

In this study, the independent variable u_l denotes three variables, i.e., u, v and p, which are displacement in x direction,

displacement in y direction and gas pressure, respectively. All the coupling relationships, which are included in those coefficients such as F_l, G_l, R_m and Γ_l, can be given based on friendly input dialogs of COMSOL Multiphysics. The COMSOL Multiphysics can solve the coupled multiphysical processes simultaneously where the cross-coupling is defined by the coupled relations between material properties and independent variables. More details about the implementation of this kind of non-linear PDEs with COMSOL Multiphysics have been presented in previous publications [19,24].

4. Numerical simulation on single-borehole blasting and enhanced gas drainage

In this section, the successive physical process for the rock fracture induced by blasting is first simulated. The blasting damage mechanism of rock is clarified, which may not only validate the numerical code but also lay basis for simulating the enhanced gas drainage when the blasting is used a method to loosen the coal seam and to increase the permeability.

4.1. Dynamic loading produced by borehole blasting

The energy stored in an explosive charge in the form of potential chemical energy is released upon detonation, partly as energy contained in the transient stress wave and partly as

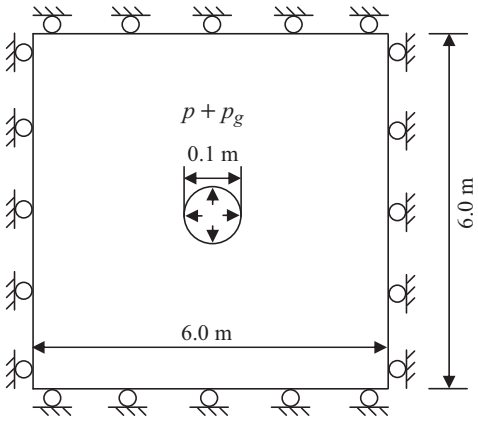

Fig. 4. Model setup for single-borehole blasting.

Table 1
Material properties of rock specimen for the numeral simulation on one-borehole blasting.

Parameter	Unit	Value
Young's modulus	GPa	70
Poisson's ratio		0.2
Mass density, ρ_s	kg/m^3	2650
Uniaxial compressive strength	MPa	157
Uniaxial tensile strength	MPa	14

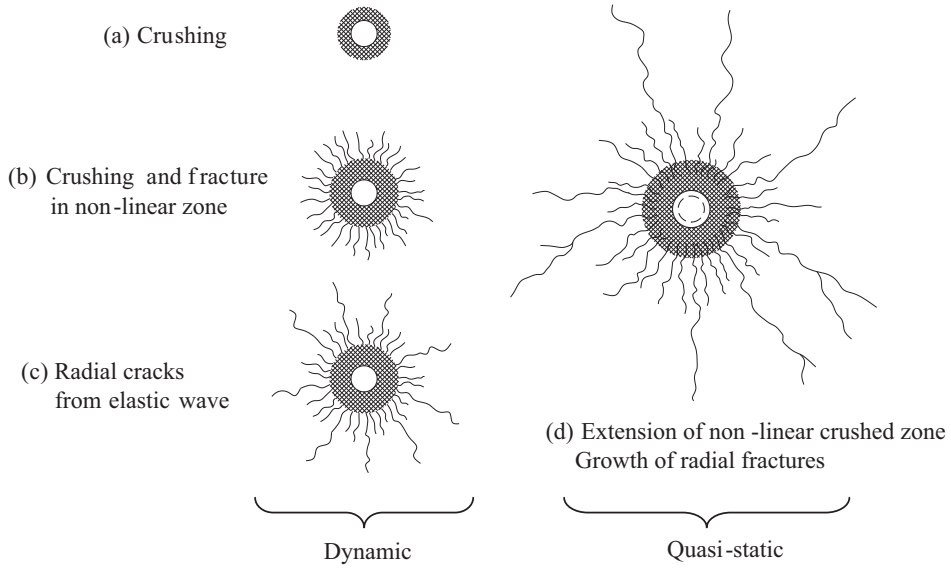

Fig. 2. The evolution of fracture patterns at the consecutive stages in the fracture process of one-borehole blasting [13].

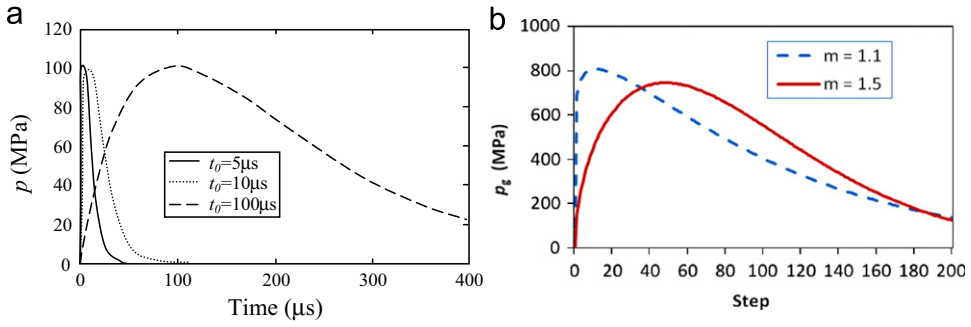

Fig. 3. Blasting stress wave and quasi-static explosion gas pressure produced by borehole blasting. (a) Stress wave ($\beta/\alpha = 1.5$) and (b) Quasi-static gas pressure.

a

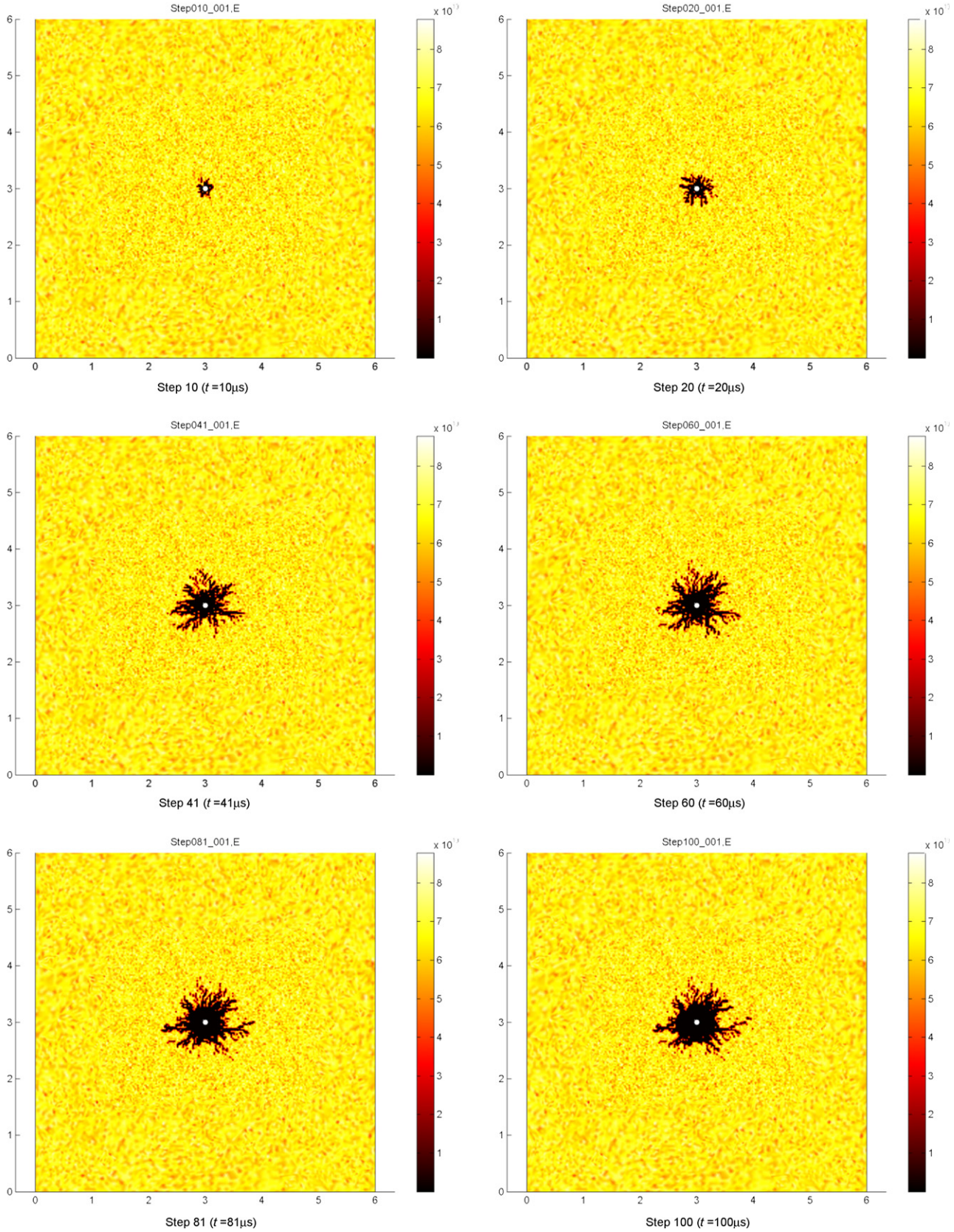

Fig. 5. The distribution of Young's modulus during the single-borehole blasting (t_0=10 μs for blasting stress wave, m=1.5 for explosion gas pressure). (a) Before blasting-induced explosion gas pressure is applied and (b) After blasting-induced explosion gas pressure is applied.

b

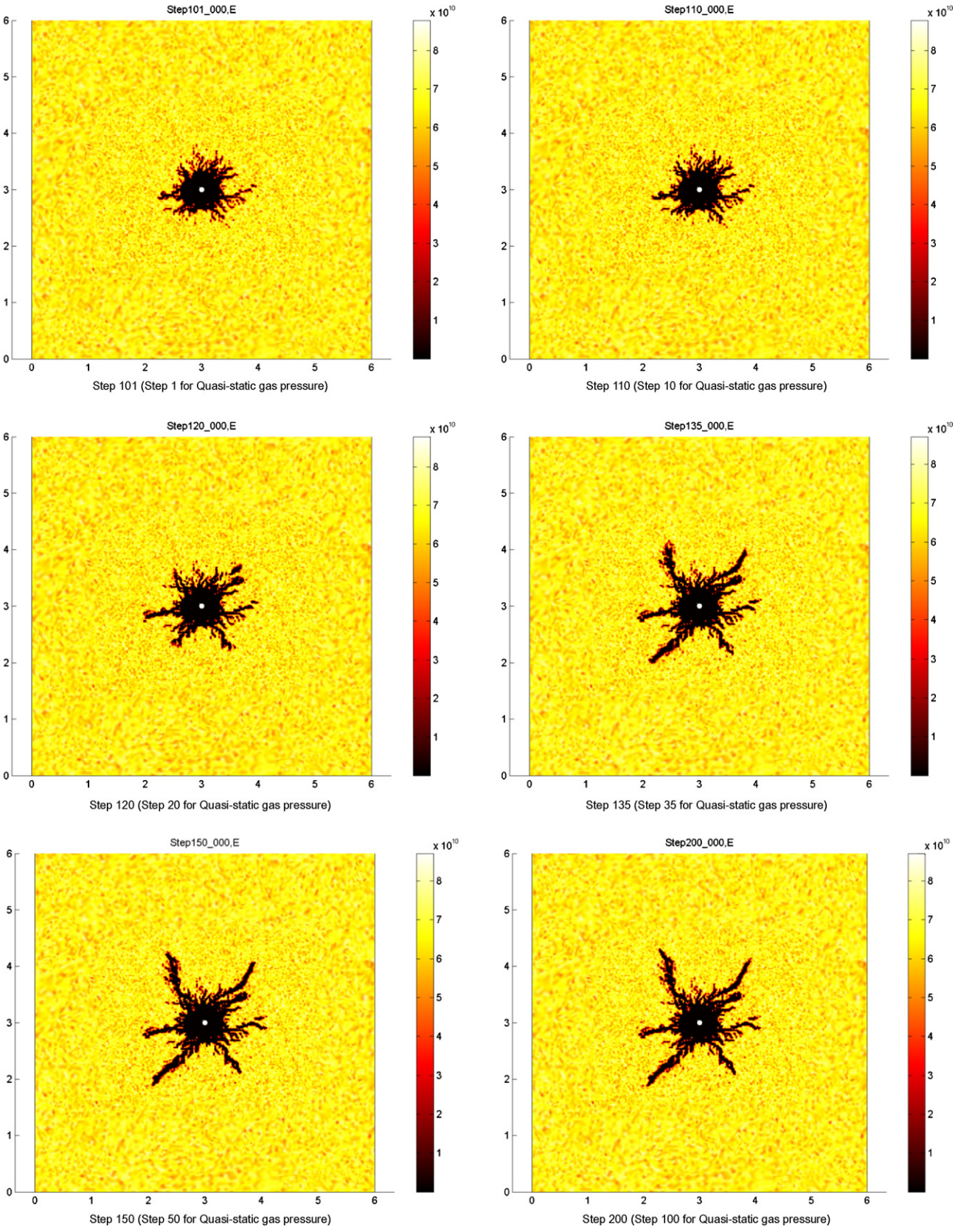

Fig. 5. Continued.

energy contained in the expanding combustion products. As proposed by Kutter and Fairhurst [13], it is the blasting stress wave and explosion gas pressure that contribute to the rock fragmentation during rock blasting. The evolution of fracture patterns associated with these intervals of loading is illustrated in Fig. 2. The blasting stress wave initiates the primarily radial cracks, and the quasi-static explosion gas pressure may result in the increase of the crushed zone radius, the extension of existing cracks and possible creation of new radial cracks. In this paper, the fracture of rock during blasting is considered to be the consecutive contribution of blasting stress wave and quasi-static explosion gas pressure. The relatively small amount of energy in the propagating stress wave indicates that the major portion of the explosive must be associated with the expanding gas [13]. The explosion gas pressure in the cavity is active for a considerably longer time than the transient stresses of the emitted wave.

In consideration of the action of blasting stress wave, as shown in Fig. 3(a), a radial stress wave as shown is applied to the boundary of the borehole. The external boundary is free. If the stress wave arrives at the boundary and is reflected, the damage pattern around the borehole will be affected by the reflected wave. In order to tackle this, in our numerical simulation the boundary is specified far away from the borehole, thus during the damage process around the borehole, the stress wave reflected from the external boundary has not arrived at the damage zone around the borehole. In this regard, viscous or non-reflection boundary is not considered in the numerical simulations.

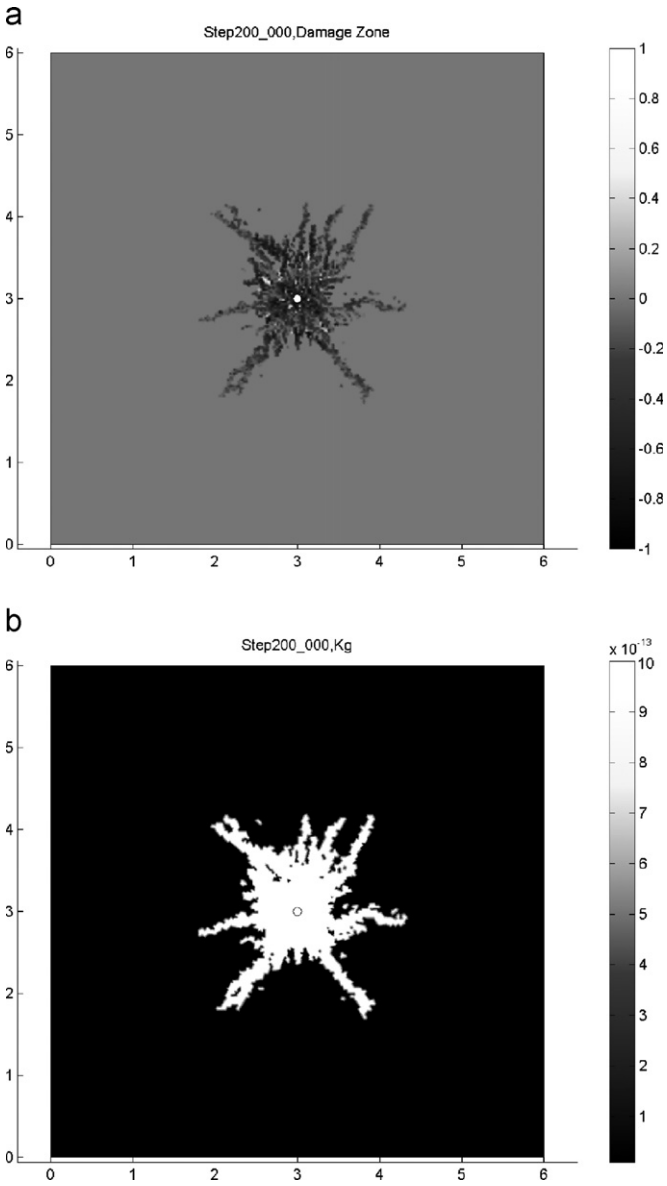

Fig. 6. The damage zone and corresponding permeability distribution after blasting for single-hole model. (a) Damage variable and (b) permeability.

The stress–time history shown in Fig. 3(a) is a general form of a pulse function, which can be used to represent a large range of the borehole pressure [12,25], expressed as,

$$p = p_0 \xi [e^{-\alpha t} - e^{-\beta t}] \tag{17}$$

where p is the stress at time t (Pa), p_0 is the peak stress (Pa), and α and β are constants. For convenient representation of the rising and decaying phases, two constants, i.e., $\xi = 1/(e^{-\alpha t_0} - e^{-\beta t_0})$ and $t_0 = (1/(\beta - \alpha))\ln(\beta/\alpha)$, are defined. In this study, the rising time t_0 is varied between 5.0, 10.0 and 100.0 μs with $\beta/\alpha = 1.5$, and the peak stress is fixed as 100.0 MPa. In this regard, the parameter t_0 is used to denote three cases of our simulations. The corresponding loadings for three cases are calculated to be 20.0, 10.0 and 1.0 MPa/s, respectively.

The stress field caused by the explosion gas pressure can be considered to be quasi-static, and has been applied at the boundary of cavity that has been enlarged resulting from blasting stress wave. In this respect, the expanding gas, i.e., quasi-static explosion gas pressure, as shown in Fig. 3b is assumed to be expressed with a Weibull function expressed as,

$$p_g(s) = p_{g0} \frac{m}{u_0} \left(\frac{s}{s_0}\right)^{m-1} \exp\left(-\left[\frac{s}{s_0}\right]^m\right) \tag{18}$$

where p_g is the explosion gas pressure (Pa), p_{g0} is the reference explosion gas pressure related to the peak value of p_g. p_{g0} is roughly specified based on previous experiences according to the equation of state of explosion products as outlined in [26], s is the loading step for explosion gas pressure, and m is a shape parameter describing the shape of this Weibull function. In Fig. 3b, the explosion gas pressures with different shape parameter m are shown, which are applied around the cavity after the blasting gas pressure. In this figure, the horizontal abscissa denotes the loading step under blasting-induced quasi-static gas pressure.

4.2. Damage zone induced by single-borehole blasting and its effect on the gas drainage

According to the numerical simulation of Ma and An [12], the geometries and loading conditions for rock specimen are shown

Table 2
Physical and mechanical parameters of coal and gas used in numerical simulation of case study.

Parameter	Unit	Value
Young's modulus of coal, E	MPa	3000
Poisson's ratio of coal, ν		0.3
Coal density, ρ_c	kg/m^3	1250
Uniaxial compressive strength of coal, f_{c0}	MPa	10
Uniaxial tensile strength of coal, f_{t0}	MPa	0.6
Internal frictional angle of coal, θ	°	38
Porosity at zero stress, ϕ_0	%	5.0
Residual porosity at high stress, ϕ_r	%	2.0
Initial coal permeability, k_0	m^2	1e-14
Biot's coefficient, α		1.0
Langmuir volume constant, a_1	m^3/kg	0.034
Langmuir pressure constant, a_2	1/MPa	1.2
Initial gas pressure, p_i	MPa	0.98
Methane dynamic viscosity, μ_g	Pa s	1.84e-5
Compressibility factor of gas, β	kg/(m^3 pa)	1.18e-5

in Fig. 4, and the material properties of rock are assigned according to Table 1. The square rock specimen is 6.0 m in side length, and the blasting hole at its center is 0.1 m in diameter. In the numerical simulations, the rock specimen is discretized into 18,460 triangular six-node finite elements, and it is simulated as a plane strain problem. Fig. 5 shows the distribution of Young's modulus in the

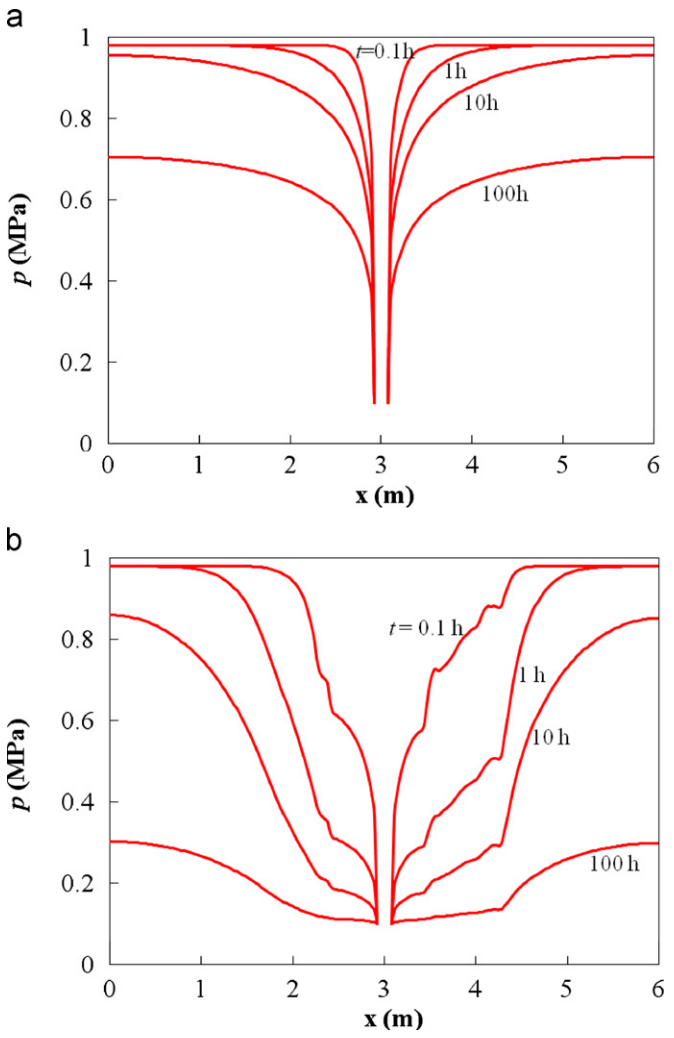

Fig. 7. Distribution of gas pressure during drainage before and after blasting for single-hole model. (a) Before destress blasting and (a) After destress blasting.

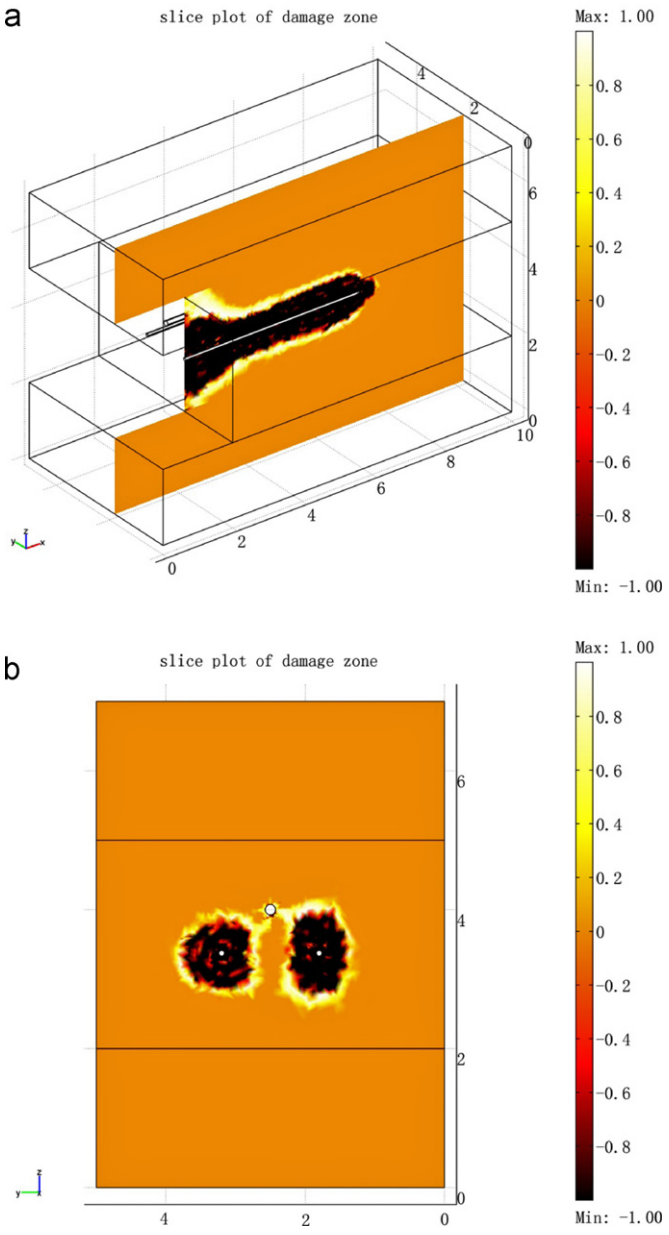

Fig. 9. Damage zone distributions after destress blasting. (a) Slice plot along the strike of blast hole and (b) y-z cross section at x = 5 m.

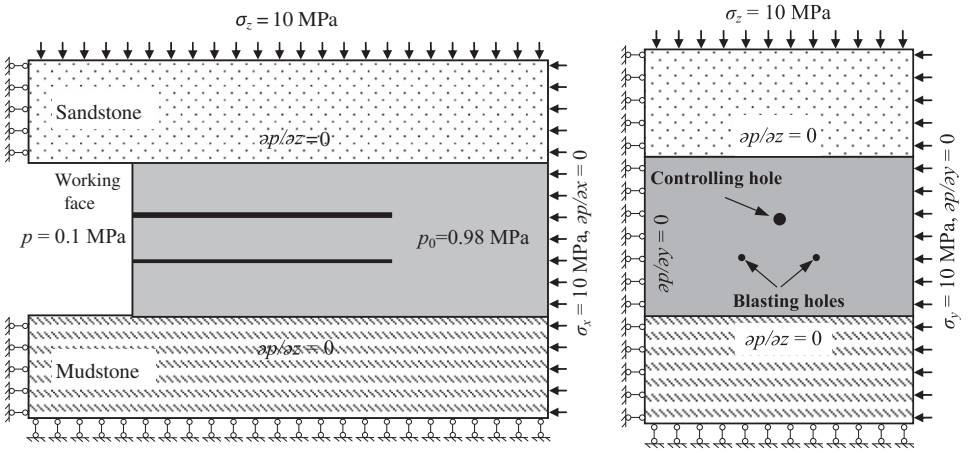

Fig. 8. Three-dimensional model and the boundary conditions for the case study.

specimen under the blasting. As given in Eq. (3), the blasting damage caused by blasting stress wave and explosion gas pressure may degrade the Young's modulus of the rock, therefore Fig. 5 can vividly show the blasting damage zone around the borehole.

When $t = 10\ \mu s$, the crushed zone is produced around the borehole, around which, the tensile radial cracks may also initiate. As time elapses, the crushed zone may extend and the radial cracks propagate further. As shown in Fig. 5b, after the quasi-static explosion gas pressure is applied, it may contribute a lot to the formation and propagation of the existing radial cracks. During the process, it is recognized, however, that the rock subjected to the explosion gas pressure has been preconditioned by stress wave impulsive loading. In this regard, the numerical model proposed above can at least qualitatively capture the damage zone development around the borehole during blasting.

In order to demonstrate the effect of blasting damage on the gas drainage, based on the damage variable as shown in Fig. 6a, which is numerically simulated for a coal specimen, the permeability is calculated and shown in Fig. 6b according to Eq. (8). The associated parameters for the gas flow in this coal specimen, such as initial permeability k_0, are listed in Table 2. Basically, the blasting-induced damage zone around the borehole corresponds to the area with increased permeability. In Fig. 6a, in order to distinctly display the two kinds of damage modes (i.e., tensile damage and shear damage), the tensile damage is represented as negative numbers, while the shear damage is represented as positive ones.

As shown in Fig. 7, because of destress blasting the gas drainage from the borehole is greatly enhanced. For example, at $t = 100$ h, the gas pressures at 1.0 m away from the borehole center before and after destress blasting are 0.64 MPa and 0.13 MPa, respectively, reflecting the much faster gas drainage due to the destress blasting.

5. Numerical simulation on a case study

As shown in Fig. 8, the numerical model is established based on the field conditions at the Chengzhuang colliery in China. The simulation domain is 10 m long, 5 m wide and 7 m high, in which the coal seams are 3 m in thickness and the working face is 3 m high with roof of sandstone and floor of mudstone. There are two blasting holes with depth of 5 m and distance of 1.4 m that are charged and detonated, while another one is only for measurement, being called controlling hole. The parameters used in this simulation are listed in Table 2.

When an explosive is detonated, a chemical reaction occurs very rapidly and a relatively small quantity of explosive is converted into gas of very high temperature. This reaction results in two types of loadings applied on the borehole wall, namely a blasting stress wave and an explosion gas pressure [13]. Because the transient analysis of the response of coal to blasting stress

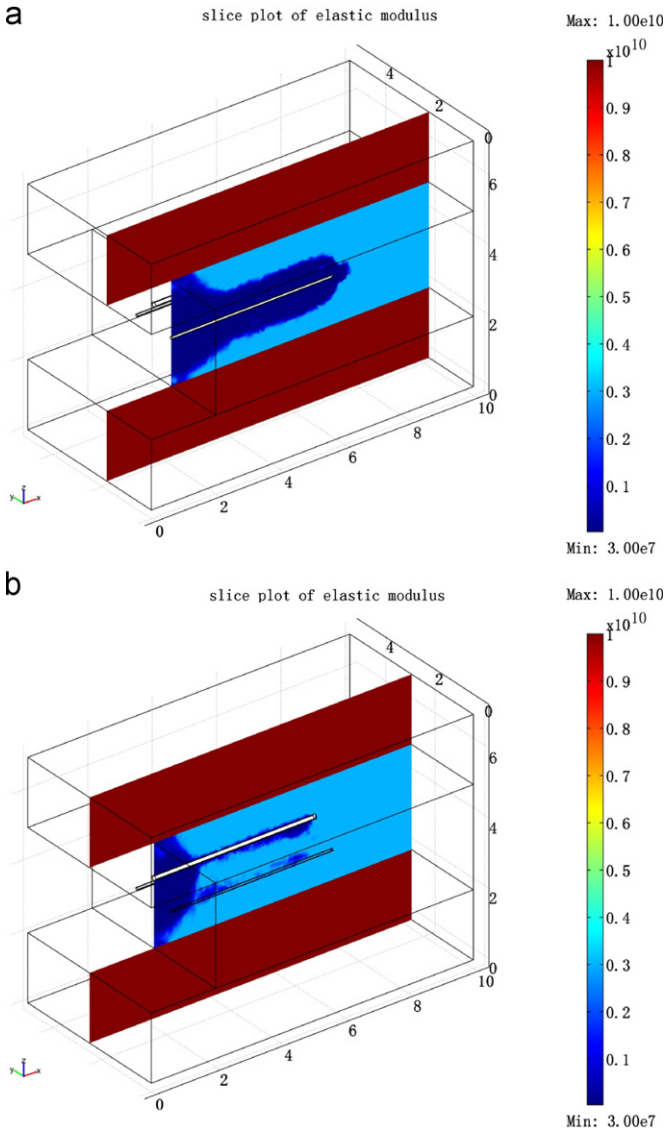

Fig. 10. Elastic modulus (in Pa) distributions in x–z cross section after destress blasting. (a) Slice plot along the strike of blasting hole, y=1.8m and (b) Slice plot along the strike of controlling hole, y=2.5m.

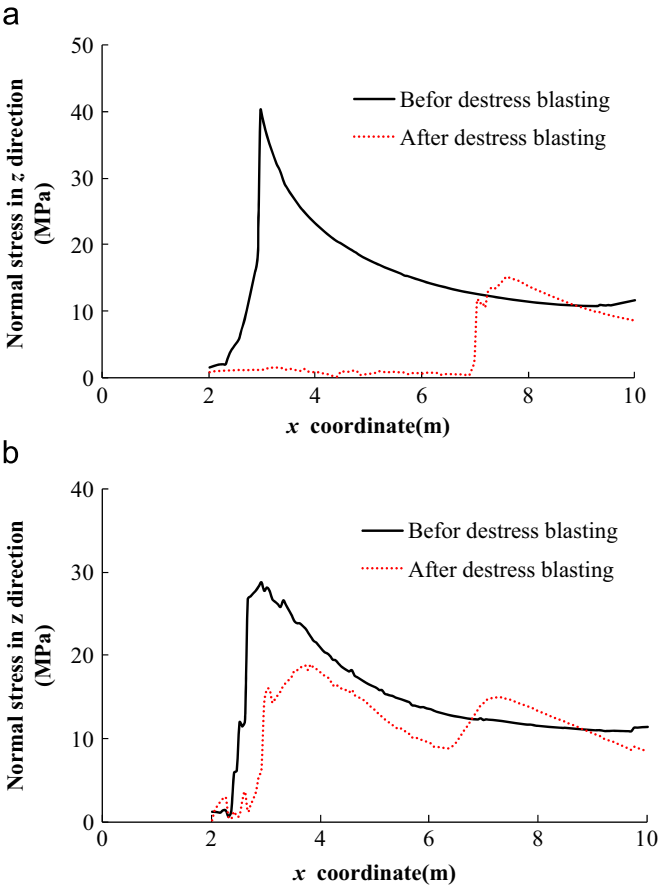

Fig. 11. Distribution of geo-stress along the strike of blasting hole and controlling hole. (a) Stress distribution at y = 1.8m, z = 3.9m and (b) Stress distribution at y = 2.5 m, z =4.5m

wave is too time-consuming and cannot afford to be simulating with PC. Therefore, for this case study, we mainly focus on the high explosion gas pressure and its impact on coalbed damage and methane migration. The value of this high explosion gas pressure can be calculated as 2275.91 MPa according to literature [26]. And then, this pressure is applied as a radial quasi-static load on the inner boundary of blasting hole in order to simulate the explosion gas pressure.

Fig. 9 shows the damage zone distribution around the working face after destress blasting. In this figure, different colors are used to denote different damage states, i.e., the white for shear damage and black for tensile damage. As shown in Fig. 9, damage zones appear around the blast hole and at the roof in front of working face which should be noticed in operation. A broken zone with radius of 0.4 m and a loosening zone with radius of 0.6 m are induced around the blasting hole.

Compared Fig. 9 to the standard blasting-induced failure pattern as illustrated in Fig. 2, it can be seen that the crushing zone is reproduced; however, the radial fracture is not successfully simulated. The reason is that the blasting stress wave is not taken into account during this numerical simulation, which may conceal the initiation of radial fractures around the expanded borehole after blasting.

Fig. 10 shows elastic modulus distributions along the strike of both blasting holes (Fig. 10a) and controlling hole (Fig. 10b). In Fig. 10a, the elastic modulus of coal seam have a notable reduction within loosening zone around the blasting hole, which accords well with damage zone distributions in Fig. 9a. However, elastic modulus around the controlling hole have no such large reduction seen in Fig. 10b, although it also basically accords with damage zone around the controlling hole shown in Fig. 9b.

Fig. 11 shows the distribution of σ_z (normal stress in z direction) along and 0.5 m above the strike of blasting hole and controlling hole before and after destress blasting, in which $x=2$ m is the working face and $x=2\sim10$ m is in coal seam. It indicates that stress concentration area transfers to deeper parts of coal seam from $x=2.8\sim5.0$ m to $x=7.0\sim9.0$ m above blasting hole and from $x=2.8\sim5.0$ m to $x=3.0\sim9.0$ m above controlling hole, respectively, as a result of elastic modulus degradation induced by blasting damage, which may be helpful for methane extraction and preventing coal and gas outbursts.

Gas (methane) pressure in coal seam is the main index for outburst proneness. Therefore, the effective measures for preventing coal and gas outburst is mainly characterized by the reduction of gas pressure. Fig. 12 shows the distribution of gas pressure along and above the strike of blasting hole (Fig. 12a) and

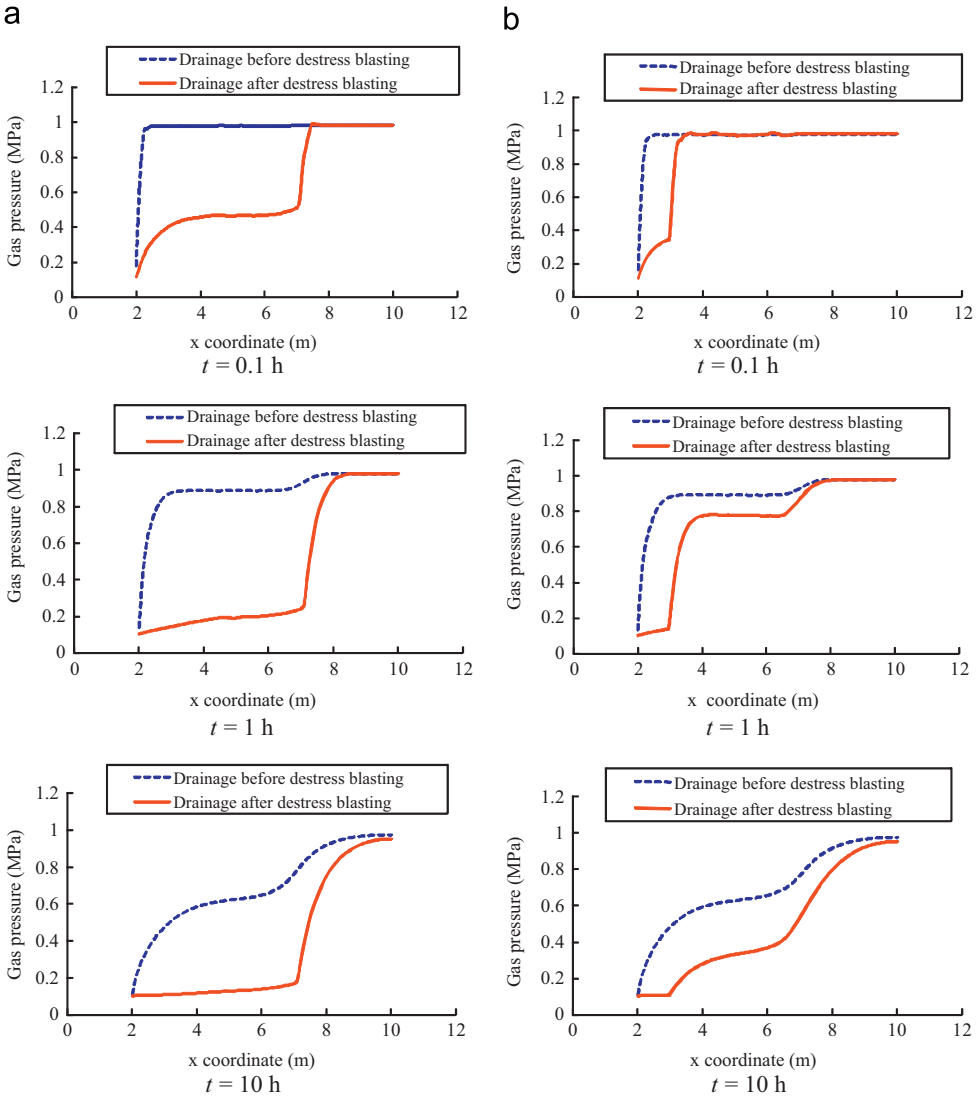

Fig. 12. Distribution of gas pressure along the strike of blasting and controlling holes at different times. (a) Gas pressure along the line at 0.5m above the blasting borehole (at y=1.8m, z=3.9m) and (b) Gas pressure along the line at 0.5 m above the controlling borehole (y=2.5m, z=4.5m).

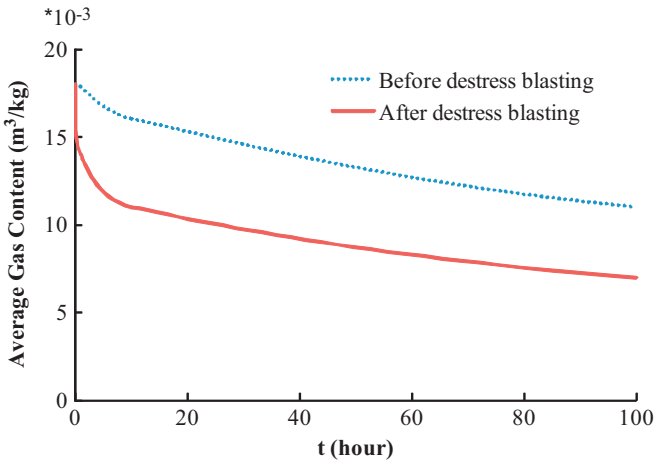

Fig. 13. Variation of average gas content in coal seam before and after destress blasting.

controlling hole (Fig. 12b). It is seen from Fig. 12a that the gas pressure declines from initial value of 0.98 MPa to about 0.2 MPa within loosening zone around the blasting hole, which accords well with damage zone distributions in Fig. 9a. The gas pressure around the controlling hole, as shown in Fig. 12b, also decreases with a fluctuating manner with the distance away from the working face. It can be concluded from Fig. 12 that destress blasting have notable effects on increasing coalbed permeability and enhancing gas drainage, especially within the loosening zone.

Fig. 13 shows the average gas content in coal seam before and after destress blasting. Basically, after destress blasting, the average gas content is smaller than those before the blasting, which indicates the salient increase of gas production after destress blasting.

6. Conclusions

It is of vital importance to understand the mechanism of gas extraction enhanced by destress blasting in order to pre-drainage methane effectively. In this work, a coupled model for coal seam damage and gas flow is used to simulate the effectiveness of destress blasting to increase coal permeability and to enhance gas extraction. The following conclusions can be drawn from the numerical simulations

The blasting damage of coal seam, together with the subsequent gas migration can be captured as a fully coupled process among coal seam damage and gas flow. In this respect, the formation of blasting damaged zone is considered as the combined contribution of blasting stress wave and quasi-static explosion gas pressure, based on which, the numerical model to simulate the blasting damage of rock is proposed.

Based on the numerical simulation on the case study of enhanced gas drainage with destress blasting of coal seam, a broken zone with radius of 0.4 m is formed around the blasting hole and a loosening zone with radius of 0.6 m is formed outside the broken zone, leading to quickly increasing coal permeability and decaying methane pressure. After the blasting, the stress concentration area is transferred to deeper parts of coal seam, i.e., extended from $x=2.8\sim5.0$ m to $x=7.0\sim9.0$ m above blasting hole and from $x=2.8\sim5.0$ m to $x=3.0\sim9.0$ m above controlling hole, respectively.

The coupled coal seam damage and gas flow model is capable of simulating the effectiveness of destress blasting to increase coal permeability and to enhance gas extraction. However, the viscous damping that may affect the simulated damage is not considered in our simulations, which should be taken into account in the further work. In addition, for the numerical simulation on the case study, only the high gas pressure produced by the detonating of explosive is taken into account. In future, the contribution of blasting stress wave to in-situ blasting damage, together with the magnitude of explosion gas pressure, needs to be examined further.

Acknowledgments

The present work is funded by National Science Foundation of China (Grant Nos. 51222401, 51128401, 50934006, and 51111130206), the Fok Ying Tung Education Foundation (Grant No.122023), Research Fund for the Doctoral Program of Higher Education of China (Grant No. 20110042110035), China-South Africa Joint Research Programme (Grant No. CS06-L01/2012DFG71060), and the Fundamental Research Funds for the Central Universities of China (Grant Nos., N110201001 and N100601004). This support is gratefully acknowledged. The authors are grateful to the reviewers for discerning comments on this paper.

References

[1] Lunarzewski LW. Gas emission prediction and recovery in underground coal mines. Int J Coal Geol 1993;35:117–45.
[2] Noack K. Control of gas emissions in underground coal mines. Int J Coal Geol 1998;35:57–82.
[3] Lu TK, Yu H, Zhou TY, Mao JS, Guo BH. Improvement of methane drainage in high gassy coal seam using waterjet technique. Int J Coal Geol 2009;79:40–8.
[4] Diamond WP, Garcia F. Prediction of longwall methane emissions: an evaluation of the influence of mining practices on gas emissions and methane control systems. In: National institute for occupational safety and health, Pittsburgh; 1999. Report of Investigations No. 9649.
[5] Wang P, Mao XB, Lin JB, Du CZ. Study of the borehole hydraulic fracturing and the principle of gas seepage in the coal seam. Proc Earth Planet Sci 2009;1:1561–73.
[6] Lu YY, Liu Y, Li XH, Kang YA. New method of drilling long boreholes in low permeability coal by improving its permeability. Int J Coal Geol 2010;84:94–102.
[7] Saharan MR, Mitri H. Destress blasting as a mines safety tool: some fundamental challenges for successful applications. Proc Eng 2011;36:37–47.
[8] Konicek P, Saharan MR, Mitri H. Destress blasting in coal mining – state-of-the-art review. Proc Eng 2011;26:179–94.
[9] Andrieux P, Hadjigeorgiou J. The destressability index methodology for the assessment of the likelihood of success of a large-scale confined destress blast in an underground mine pillar. Int J Rock Mech Min Sci 2008;45(3):407–21.
[10] Liu JC, Wang HT, Yuan ZG, Fan XG. Experimental study of pre-splitting blasting enhancing pre-drainage rate of low permeability heading face. Proc Eng 2011;26:818–23.
[11] Huang BX, Liu CY, Fu JH, Guan H. Hydraulic fracturing after water pressure control blasting for increased fracturing. Int J Rock Mech Min Sci 2011;48(6):976–83.
[12] Ma GW, An XM. Numerical simulation of blasting-induced rock fractures. Int J Rock Mech Min Sci 2008;45:966–75.
[13] Kutter HK, Fairhurst C. On the fracture process in blasting. Int J Rock Mech Min Sci 1971;8:181–202.
[14] Bhandari S. On the role of stress waves and quasi-static gas pressure in rock fragmentation by blasting. Acta Astronautica 1979;6:365–83.
[15] Swenson DV, Taylor LM. A finite element model for the analysis of tailored pulse stimulation of boreholes. Int J Numer Anal Meth Geomech 1983;7(4):469–84.
[16] Esena S, Onederraa I, Bilgin HA. Modelling the size of the crushed zone around a blasthole. Int J Rock Mech Min Sci 2003;40:485–95.
[17] Wei XY, Zhao ZY, Gua J. Numerical simulations of rock mass damage induced by underground explosion. Int J Rock Mech Min Sci 2009;46:1206–13.
[18] Young GBC. Computer modelling and simulation of coalbed methane resources. Int J Coal Geol 1998;35:369–79.
[19] Zhu WC, Liu J, Sheng JC, Elsworth D. Analysis of coupled gas flow and deformation process with desorption and Klinkenberg effects in coal seams. Int J Rock Mech Min Sci 2007;44(7):971–80.
[20] Connell LD. Coupled flow and geomechanical processes during gas production from coal seams. Int J Coal Geol 2009;79(1-2):18–28.
[21] Karacan CÖ, Diamond WP, Schatzel SJ. Numerical analysis of the influence of in-seam horizontal methane drainage boreholes on longwall fact emission rates. Int J Coal Geol 2007;72:15–32.

[22] Zhu WC, Tang CA. Micromechanical model for simulating the fracture process of rock. Rock Mech Rock Eng 2004;37(1):25–56.
[23] COMSOL AB. COMSOL multiphysics version 3.5, user's guide and reference guide. (ww.comsol.com). (2008).
[24] Zhu WC, Wei CH, Liu J, Qu HY, Elsworth D. A model of coal-gas interaction under variable temperatures. Int J Coal Geol 2011;86(2-3):213–21.
[25] Cho SH, Kaneko K. Influence of the applied pressure waveform on the dynamic fracture processes in rock. Int J Rock Mech Min Sci 2004;41:771–84.
[26] Persson PA, Holmberg R, Lee J. Rock blasting and explosives engineering. CRC Press; 1994 p. 100–142.